SINTEF
PROCEEDINGS
1

Selected papers from 10th International Conference on Computational Fluid Dynamics in the Oil & Gas, Metallurgical and Process Industries

Progress in Applied CFD

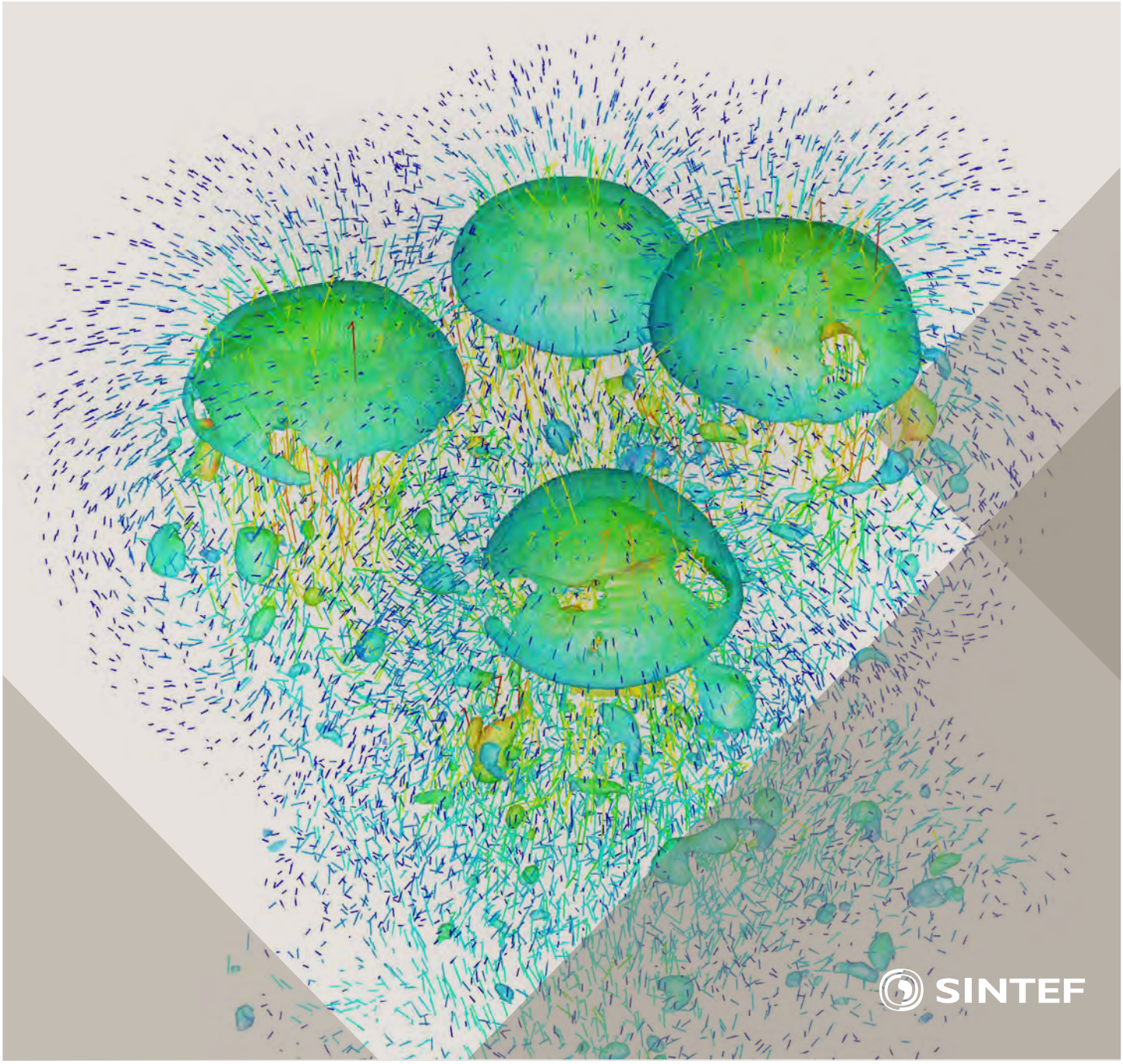

SINTEF Proceedings

Editors:
Jan Erik Olsen and Stein Tore Johansen

Progress in Applied CFD

Selected papers from 10th International Conference on Computational Fluid Dynamics in the Oil & Gas, Metallurgical and Process Industries

SINTEF Academic Press

SINTEF Proceedings no 1
Editors: Jan Erik Olsen and Stein Tore Johansen
Progress in Applied CFD
Selected papers from 10th International Conference on Computational Fluid Dynamics in the Oil & Gas, Metallurgical and Process Industries

Key words:
CFD, Flow, Modelling

Cover, illustration: Rising bubbles by Schalk Cloete

ISSN 2387-4287 (printed)
ISSN 2387-4295 (online)
ISBN 978-82-536-1432-8 (printed)
ISBN 978-82-536-1433-5 (pdf)

60 copies printed by AIT AS e-dit
Content: 100 g munken polar
Cover: 240 g trucard

SINTEF Academic Press
Address: Forskningsveien 3 B
PO Box 124 Blindern
N-0314 OSLO
Tel: +47 22 96 55 55
Fax: +47 22 96 55 08

www.sintef.no/byggforsk
www.sintefbok.no

SINTEF Proceedings
SINTEF Proceedings is a serial publication for peer-reviewed conference proceedings on a variety of scientific topics.
The processes of peer-reviewing of papers published in SINTEF Proceedings are administered by the conference organizers and proceedings editors. Detailed procedures will vary according to custom and practice in each scientific community.

PREFACE

This book contains selected papers from the 10th International Conference on Computational Fluid Dynamics in the Oil & Gas, Metallurgical and Process Industries. The conference was hosted by SINTEF in Trondheim in June 2014 and is also known as CFD2014 for short. The conference series was initiated by CSIRO and Phil Schwarz in 1997. So far the conference has been alternating between CSIRO in Melbourne and SINTEF in Trondheim. The conferences focus on the application of CFD in the oil and gas industries, metal production, mineral processing, power generation, chemicals and other process industries. The papers in the conference proceedings and this book demonstrate the current progress in applied CFD.

The conference papers undergo a review process involving two experts. Only papers accepted by the reviewers are presented in the conference proceedings. More than 100 papers were presented at the conference. Of these papers, 27 were chosen for this book and reviewed once more before being approved. These are well received papers fitting the scope of the book which has a slightly more focused scope than the conference. As many other good papers were presented at the conference, the interested reader is also encouraged to study the proceedings of the conference.

The organizing committee would like to thank everyone who has helped with paper review, those who promoted the conference and all authors who have submitted scientific contributions. We are also grateful for the support from the conference sponsors: FACE (the multiphase flow assurance centre), Total, ANSYS, CD-Adapco, Ascomp, Statoil and Elkem.

Stein Tore Johansen & Jan Erik Olsen

Organizing committee:

Conference chairman: Prof. Stein Tore Johansen
Conference coordinator: Dr. Jan Erik Olsen
Dr. Kristian Etienne Einarsrud
Dr. Shahriar Amini
Dr. Ernst Meese
Dr. Paal Skjetne
Dr. Martin Larsson
Dr. Peter Witt, CSIRO

Scientific committee:

J.A.M.Kuipers, TU Eindhoven
Olivier Simonin, IMFT/INP Toulouse
Akio Tomiyama, Kobe University
Sanjoy Banerjee, City College of New York
Phil Schwarz, CSIRO
Harald Laux, Osram
Josip Zoric, SINTEF
Jos Derksen, University of Aberdeen
Dieter Bothe, TU Darmstadt
Dmitry Eskin, Schlumberger
Djamel Lakehal, ASCOMP
Pär Jonsson, KTH
Ruben Shulkes, Statoil
Chris Thompson, Cranfield University
Jinghai Li, Chinese Academy of Science
Stefan Pirker, Johannes Kepler Univ.
Bernhard Müller, NTNU
Stein Tore Johansen, SINTEF
Markus Braun, ANSYS

CONTENTS

LATTICE BOLTZMANN SIMULATIONS APPLIED TO UNDERSTANDING THE STABILITY OF MULTIPHASE FLUID INTERFACES

Gerald G PEREIRA*
CSIRO, Computational Modelling Group, Clayton 3169, AUSTRALIA

* E-mail: Gerald.Pereira@csiro.au

ABSTRACT

Multiphase flow occurs in a multitude of industrial and technological situations ranging from oil and minerals recovery to microfluidics and nanofluidics. In all these cases we are interested in modelling the flow of two immiscible phases through a complex geometrical domain. In the past few years, the Lattice Boltzmann method has been developed to model fluid flow both for single phase flow and two (or more) phases. In this study we consider the flow of a less viscous phase into a more viscous fluid (say water into oil) and focus on the stability of the interface. In particular it is known the interface becomes unstable leading to fingers of the less viscous phase jetting through the more viscous phase which has deleterious effects on oil recovery. We use the LB method to model this flow for a variety of fluid geometries.

Keywords: Multiphase, interface stability, oil and gas.

NOMENCLATURE

Greek Symbols

ρ LB particle density, [dimensionless].
μ LB dynamic viscosity, [dimensionless].
ν LB Kinematic viscosity, [dimensionless].

Latin Symbols

f LB distribution function, [dimensionless].
P LB pressure, [dimensionless].
$\boldsymbol{r}$ LB lattice position, [dimensionless].
$\boldsymbol{u}$ LB velocity, [dimensionless].
$\boldsymbol{e}$ LB discrete velocity vectors, [dimensionless].
F LB force, [dimensionless].
g LB weights, [dimensionless].
c_s LB speed of sound, [dimensionless].
w LB weights, [dimensionless].

Sub/superscripts

k multiphase component.
i LB velocity direction.

INTRODUCTION

Understanding immiscible multiphase flow is vital in a vast array of industries such as oil recovery, mining, and technologies such as micro or nanofluidics. In our work we have been most interested in applications in the oil and gas industries where initially the rock or *porous medium* is filled with a wetting (oil phase). A second, non-wetting phase (i.e. water) is then injected to displace the wetting phase. Since the two phases are immiscible a well defined interface exists between the two phases.

One of the most important quantities to determine the capability of a porous medium to produce oil is the permeability. When there are two (or more) phases present relative permeability curves are determined. In this case, as the second phase is injected instabilities in the interface between the two fluids can cause trapping of the initial phase by the injected phase. As such the relative permeability of the initial phase falls rapidly, even though there may be a large amount of that phase still present in the porous medium.

Although relative permeabilities can be measured experimentally this can be quite difficult and time and/or money consuming. Alternatively , if one can obtain a digital model (such as from computed tomography X-ray scans or CT scans) of the rock at the pore level then this data may be imported into suitable numerical solvers so as to solve for the transport properties in the porous medium. There are a number of numerical methods which may, in principal, solve for the flow field in a real porous media. For example, in the past network models (Blunt, 2001; Pereira, 1999) have been used to determine relative permeability curves. In this case the complex topology of the porous medium is approximated by an equivalent network of interconnected pores and throats. The pores hold most of the fluid while the throats are where most of the pressure drops occur. Pores are approximated as spheres (or some similar regular geometry) while the throats are approximated by long, thin cylinders. Although relative permeability curves can be calculated with this method, the biggest problem is to accurately represent the complex topological microstructure with much simpler network models. Invariably, this leads to over-simplifications of the porous medium which then lead to results which are not representative of the real medium.

Alternatively, one can directly apply the numerical CFD solver to the CT data and solve for the (steady-state) flow field. Using techniques such as finite element methods or Smoothed Particle Hydrodynamics one requires a suitable boundary mesh between the void space and solid domain of the porous medium. Because

this is a highly irregular surface, this is typically very difficult. A relatively recent CFD method that overcomes many of the problems with the methods mentioned above is the Lattice Boltzmann (LB) method (Succi, 2001). This method is based on the Boltzmann transport equation which considers the microscopic motion of distributions of particles. In the LB method the velocity space is discretised (and limited) to a small subset of possibilities, which enables a solution on a suitable simplified lattice. However, the exact pore space that is present in the digital data is modelled, i.e. the resolution of the numerical model is at the same scale as the digital data with no approximations.

The LB method is now quite commonly used to compute flow fields for single phase flow (Pan and Miller, 2006). However, its application to immiscible multiphase flow is much more in its infancy. The main question to address is how to capture the effect of surface tension which causes the separation of the two phases? There have been a number of different attempts at representing the effect of surface tension. These include a colour gradient model (Gunstensen and Rothmann, 1992) a thermodynamic, free energy model (Swift *et al*, 1995) a mean-field theory model (He *et al*, 1998) and a microscopic interaction model based on attractive and/or repulsive potentials between neighbouring particles (Shan and Chen, 1993). The methods by Swift *et al* (1995) and He *et al* (1998) were developed to naturally model a change of phase whereas the other two methods are isothermal and so specifically model the two-phase (immiscible) region of phase space. In this study we adopt the so called *Shan-Chen model* (Shan and Chen, 1993) to model surface tension. However, we implement an enhanced version of this model, so to reduce a numerical artefact - the so-called *spurious currents*.

In the next section we introduce this model and extract macroscopic parameters such as surface tension and contact angles from it. We then apply it to sample porous media such as packed beds and carbonate samples.

MODEL DESCRIPTION

The LB model is a mesoscopic numerical method used to study incompressible fluid dynamics. Its main advantages over more conventional CFD techniques (which directly solve the Navier-Stokes equations) are its programming simplicity, computational efficiency and inherent parallelism due to a large amount of local computations. In addition, as mentioned in the Introduction, it naturally deals with complex porous media if suitable digital information is provided. Details of this method, applied to single phase flow, are available (Succi, 2001; Chen and Doolen, 1998) and thus we shall only focus here on the LB method applied to immiscible, multiphase flow.

In the LB method distributions of fluid particles are propagated on a discrete lattice. At each time-step the fluid particles undergo a two-step process where particles are propagated to adjacent lattice nodes (called "*streaming*") and then collided with other particles which converge on a specific node (called "*collision*"). Solid boundaries are treated in the streaming step whereby a bounce-back boundary condition is implemented (i.e. any fluid particles which stream into a solid site are simply reversed). More complex and accurate boundary conditions such as half-way bounce-back or linear interpolation boundary conditions are also possible. In the collision step particle distributions relax towards a given equilibrium distribution - a Maxwellian distribution. Then macroscopic properties such as fluid density, fluid velocity and the stress tensor can be derived from the particle distributions. If we are dealing with only a single fluid, one set of particle distributions is defined, i.e. $f(\boldsymbol{r}, \boldsymbol{u}, t)$ which denotes the distribution of particles travelling with a particular velocity $\boldsymbol{u}$ at time t at lattice node $\boldsymbol{r}$. We will only consider a three dimensional (3D) model in this paper so that we implement the common D3Q19 model which indicates that there are 18 possible vectors, $\boldsymbol{e}_i$, in which particles may move in addition to the null vector. These 18 possibilities are the vectors ($\pm$1, 0, 0), (0,$\pm$1,0), (0,0,$\pm$1), ($\pm$1,$\pm$1,0), ($\pm$1,0,$\pm$1), (0,$\pm$1,$\pm$1).

For n phases we now define n sets of distributions functions, which represent each immiscible phase - $f^1(\boldsymbol{r},\boldsymbol{u},t)$ ... $f^n(\boldsymbol{r},\boldsymbol{u},t)$. For each phase we solve the LB equation at node i. So for the k^{th} phase (where $k \in 1,...n$) we need to solve the LB equation:

$$f_i^k(\boldsymbol{r}+\boldsymbol{e}_i\Delta t, t+\Delta t) - f_i^k(\boldsymbol{r},t) = -\frac{1}{\tau_k}\left[f_i^k(\boldsymbol{r},t) - f_i^{k,eq}(\boldsymbol{r},t)\right]. \quad (1)$$

The term $f_i^{k,eq}$ is the equilibrium Maxwell distribution given by

$$f_i^k = w_i\rho_k\left[1+\frac{\boldsymbol{e}_i\bullet\boldsymbol{u}_k^{eq}}{c_s^2}+\frac{(\boldsymbol{e}_i\bullet\boldsymbol{u}_k^{eq})^2}{2c_s^4}-\frac{\boldsymbol{u}_k^{eq}\bullet\boldsymbol{u}_k^{eq}}{2c_s^2}\right], \quad (2)$$

where w_i are weights which are defined for the given D3Q19 model. In Eq.(1), τ_k represents a relaxation time for phase k and it can be shown to be related to kinematic viscosity via $\nu_k = c_s^2(\tau_k - 1/2)$ where c_s is the sound speed and c_s^2 equals 1/3.

The relationship to macroscopic parameters such as density and velocity of the k^{th} phase are given by

$$\rho_k = \sum_i f_i^k \quad \text{and} \quad \rho_k\boldsymbol{u}_k = \sum_i f_i^k\boldsymbol{e}_i. \quad (3)$$

The Shan-Chen model (Shan and Chen, 1993) (also referred to sometimes as the *pseudo-potential* model) employs nearest neighbour inter-particle potentials to model the interactions between components. In a sense this follows physical reality at the microscopic level where molecules interact via short-range Lennard-Jones type potentials. In the Shan-Chen model lattice nodes which have a separation of less than or equal to $2^{1/2}$ units are coupled together.

In the Shan-Chen model, the interaction potential between components is accommodated via a force, F_k which is introduced through the velocity $\boldsymbol{u}_k^{eq}$ in Eq.(2). This velocity is defined as (Shan and Chen, 1993)

$$\rho_k\boldsymbol{u}_k^{eq} = \rho_k\boldsymbol{u}' + \tau_k\boldsymbol{F}_k. \quad (4)$$

In this equation $\boldsymbol{u}'$ is a combined velocity and to satisfy momentum conservation must be

$$\boldsymbol{u}' = \frac{\sum_k \tau_k^{-1} \rho_k \boldsymbol{u}_k}{\sum_k \tau_k^{-1} \rho_k} \quad . \qquad (5)$$

The fluid-fluid interaction for phase k at lattice node $\boldsymbol{r}$ is then given by

$$\boldsymbol{F}_k(\boldsymbol{r}) = \rho_k(\boldsymbol{r}) c_s^2 \sum_{k \neq k'} g_{kk'} \sum_i w(|\boldsymbol{e}_i|^2) \times \rho_{k'}(\boldsymbol{r} + \boldsymbol{e}_i)\boldsymbol{e}_i \ , \qquad (6)$$

where $g_{kk'}$ is the interaction potential (or coupling parameter) between dissimilar components. The weights w depend on the separation between interacting nodes with $w(1)=1/6$ and $w(2)=1/12$. Note, we assume the coupling is zero for similar components. The pressure in this model is given by the equation of state

$$P = c_s^2 \sum_k \rho_k + 3 \sum_{kk'} g_{kk'} \rho_k \rho_{k'} \ . \qquad (7)$$

One of the issues with this nearest neighbour implementation is that it leads to large spurious currents which are a numerical artefact. These numerical artefacts, if not reduced to a minimum, will lead to large numerical instabilities. Thus we shall attempt to reduce these numerical instabilities in two ways. Firstly, it has been found (Porter *et al*, 2012) extending the range of the pseudo-potential leads to a significant reduction (up to 1000 times) of these spurious currents. The range of pseudo-potential can in principal go to infinity but this of course comes at a computational cost. We have implemented here both 6th order (including all neighbours less than or equal to 2 units away) and 8th order (including all neighbours less than or equal to $8^{1/2}$ units away) pseudo-potentials. This increases the number of neighbours to be sampled from 18 (Shan-Chen) to 32 (6^{th} order) to 64 (8^{th} order), but greatly enhances the numerical stability of the method. Weights, which are required in Eq. (6), for the additional neighbour pairs have been given by Sbragaglia *et al* (2007). Secondly, a slightly different form of the LB evolution (Eq.1) is used which employs an explicit force in the LB equation. This forcing term is defined by He *et al* (1998)

$$\Im_i^k = \frac{F_k \bullet (\boldsymbol{e}_i - \boldsymbol{u}^{eq})}{\rho_k c_s^2} f_i^{k,eq} \ , \qquad (8)$$

where now $\boldsymbol{u}^{eq} = \boldsymbol{u}'$ and $\Im_i^k$ is suitably added to Eq.(1). The phase velocities are modified in this case to $\rho_k \boldsymbol{u}_k = \sum_i f_i^k \boldsymbol{e}_i + \boldsymbol{F}_k/2$.

Relationship to macroscopic surface tension

The Shan-Chen model yields an interface between two immiscible phases via microscopic parameters g_{12}, g_{s1} and g_{s2}. (The subscript s refers to a solid surface so that g_{s1} is the interaction between solid surface and phase 1.) They need to be related to macroscopic surface tension and contact angle measurements. To do this we use the Young-Laplace equation

$$\Delta P = \frac{2\gamma}{R}, \qquad (9)$$

where γ is the macroscopic surface tension and R is a droplet radius.

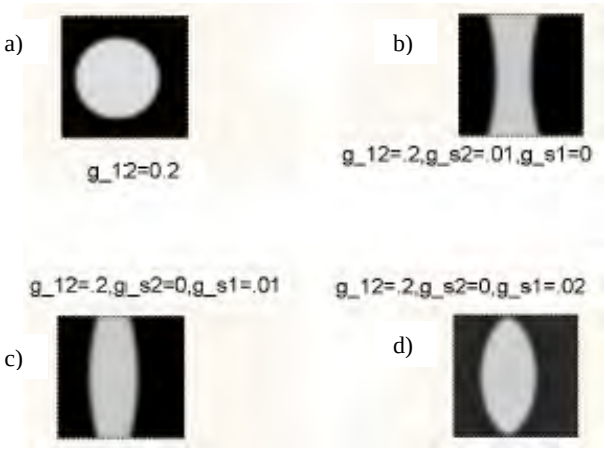

Figure 1. Droplets created using the Shan-Chen model (a) In the bulk, (b) wetting droplet (light shade) between two hard, flat surfaces (c) non-wetting droplet between surfaces and (d) different contact angle non-wetting drop between two surfaces.

To obtain γ we begin with a number of different sized cubical droplets. These quickly relax to spheres of different radius (see Fig. 1a) and then we measure the pressure difference between the interior and exterior of the droplet using Eq. (7). This plot is shown in Fig. 2 and the surface tension is extracted from the gradient. To convert this surface tension to physical (SI) units we need to suitably scale it with physical values of mass and time. Properties such as length and mass can be easily related to physical case of interest. However, time is more difficult. A time scale can be extracted by relating the physical viscosity and LB viscosity.

We can also model different contact angles of droplets on hard surfaces as shown in Fig.1b, c and d. This is done by varying the surface-droplet parameters g_{s1} and g_{s2}. In Fig. 1b these parameters are set to $g_{s1} = 0.01$ and $g_{s2} = 0.0$ resulting in a wetting droplet (the light shade corresponds to the droplet). In Figs. 1c and 1d we change these parameters to $g_{s1} = 0.0$ and $g_{s2} = 0.01$ (for c) and $g_{s1} = 0.0$ and $g_{s2} = 0.02$ (for d) resulting in different non-wetting contact angles. A relationship relating the contact to the interaction (coupling) constants has been given by Huang *et al* (2007):

$$\cos\theta = \frac{2(g_{s1} - g_{s2})}{g_{12}(\rho_1 - \rho_2)}, \qquad (10)$$

where ρ_1 and ρ_2 are densities of fluid 1 and 2, respectively.

It is well know that the Shan-Chen model gives surface tensions which can depend on the viscosity ratio between fluids. This can be overcome by using multi-relaxation time (MRT) schemes (D'Humieres *et al*, 2002). However, for the present study we implement a single relaxation time (SRT) scheme.

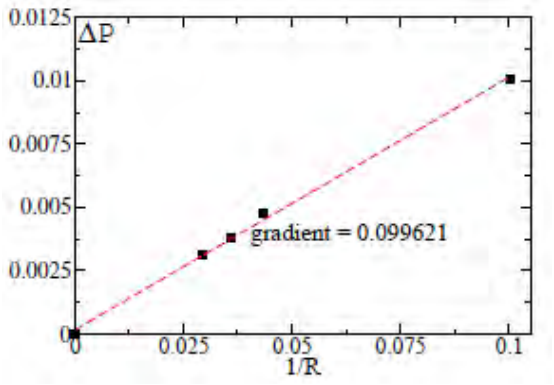

Figure 2. Young-Laplace law for g_{12} = 0.2. We plot the pressure difference between the interior and exterior of the droplet versus the inverse radius of the droplet. Black squares represent the LB results while the dashed line is a best fit line which passes through the origin and the squares.

IMMISCIBLE FLUID DISPLACEMENT

We next apply the LB model to flow in a square capillary or tube. The tube is initially filled with a wetting fluid and a second non-wetting fluid is injected to displace the wetting fluid. This can be achieved in one of two ways - either with an inlet and outlet pressure difference or with a body force (such as gravity) on the whole fluid. The pressure boundary conditions are implemented by prescribing densities (via the distribution functions) on the inlet and outlet (Zou and He, 1997). Body forces can be included by adding them to the force in Eq. (4). A number of different viscosity ratios have been implemented in the following simulations. Generally, we only obtain numerically stable simulations for viscosity ratios between 1 and 5. The non-wetting fluid has the lower viscosity so as to mimic the (practical) case of a water-oil flood.

Capillary pressure

When a non-wetting fluid displaces a wetting fluid in a capillary tube it must overcome the capillary pressure given by $2\gamma\cos\theta/R$ where $2R$ is the tube cross-sectional diameter. So for a given pressure difference between the inlet and outlet the non-wetting fluid will only enter the tube with a diameter greater than $2\gamma\cos\theta/\Delta P$. To test that the model captures this correctly we ran a number of simulations with a narrow, rectangular throat joining the inlet and outlet reservoirs. (The inlet is at the left edge of Fig. 3 and outlet is at the right edge of this figure. The invading fluid is the A-phase which is red.) For each simulation the throat width is constant (at 20 LB units) but the pressure gradient is successively decreased. In Figs. 3a-3d we show the results where we have decreased the pressure difference between the inlet and outlet from 10^{-2} LB units (Fig. 3a) to 5.8 X 10^{-3} (Fig. 3b) to 5.1 X 10^{-3} (Fig. 3c) and finally 4.4 X 10^{-3} (Fig. 3d).

In Fig.3a the invading, non-wetting fluid (red) rapidly invades the narrow throat before entering the outlet reservoir and increasing in size as a non-wetting bubble. In Fig.3b the invading fluid can overcome the capillary threshold pressure but by Fig. 3c this is not possible. We thus estimate the threshold capillary pressure is between 5.1 X 10^{-3} and 5.8 X 10^{-3} LB units. Additional simulations in between these two values have been carried out and it appears that the threshold pressure is very near 5.1 X 10^{-3} LB units. Note in Figs. 3c and 3d the meniscus in the left-hand (inlet) reservoir cannot fill the corners as the pressure in the A-phase (red region) is not large enough to fill the small corner. In both these cases, even though we ran the simulation for as long as possible, the A-phase never filled the narrow throat or the corner regions.

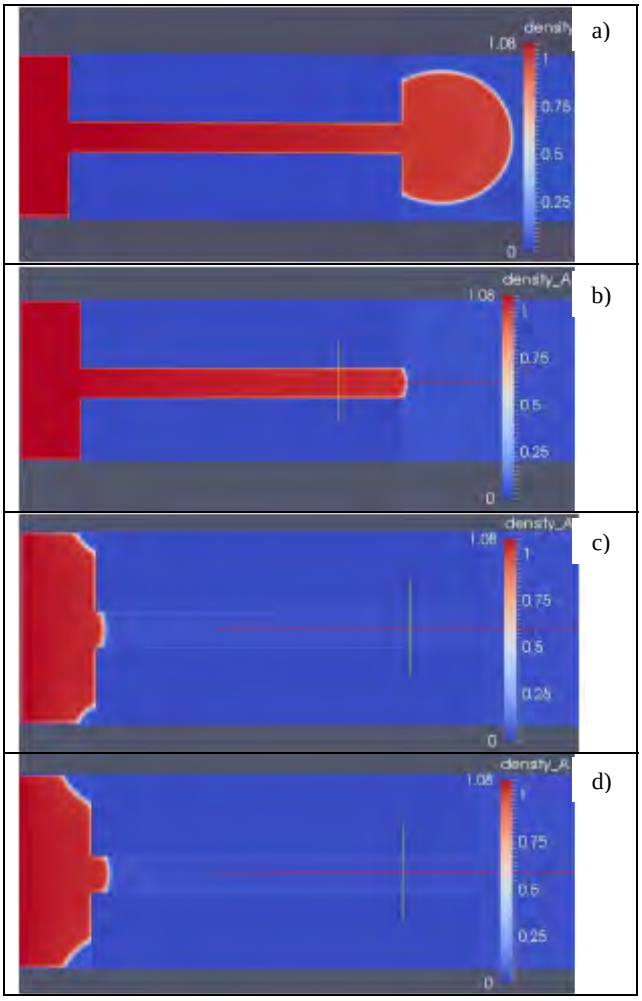

Figure 3. LB simulations of a non-wetting fluid (red) invading a rectangular pore throat which is 20 LB units wide. a) A pressure difference of 10^{-2} LB units between inlet (left side) and outlet (right side) has been applied. b) Pressure difference of 5.8 X 10^{-3}, c) pressure difference of 5.1 X 10^{-3} and d) pressure difference of 4.4 X 10^{-3}. For the last two cases, the meniscus remains at the entrance of the narrow throat for the duration of the simulations (which were allowed to run for as long as practically possible).

Porous media

The aim of this work is to be able to model multiphase flow in a real porous medium. Previously we have done this for single phase flow in carbonate rocks using CT scan digital data (Liu *et al*, 2014). Multiphase flow poses a much larger numerical problem due to surface tension which causes the two phases to remain demixed. Applying the present model directly to CT data is a serious problem for a number of reasons. Firstly, the

complex and irregular pore space can lead to extremely narrow throats and hence extremely high pressures. The multiphase LB algorithm becomes numerically unstable very quickly and the solution cannot be achieved. Secondly, the multiphase method requires one to solve for up to *n* distribution functions which can mean an exorbitantly large amount of compute time and memory. Thirdly the complex 3D topology of real porous media makes it extremely difficult to visualize and (hence) understand the flow transport paths.

For the reasons just mentioned, initially, we implement a much simpler porous medium and then build to more complex cases. These are pseudo 3D models. We previously (Pereira, 1999) used these types of model to understand the rules for three-phase displacement (i.e., displacement of oil and water by a third phase such as gas). Although they are an over-simplification of a real porous medium, they are extremely useful in developing new numerical models since they allow us to follow the pore-scale fluid flow.

The sample porous medium we use is a rectangular domain (in the *x* and *y* directions) with a small thickness (in the third direction, *z*). The length of the sample in the *x* direction is slightly greater than in the *y* direction. Solid spheres are placed in a two-dimensional, hexagonal pattern in the rectangular domain. The spheres have a variable diameter selected from a uniform distribution between 4 and 10 LB units. The centres of the spheres coincide with the mid-plane in the *z*-direction. Figure 4 shows the sample porous medium with the inlet placed along the bottom edge and the outlet along the top edge. Solid spheres are a dark blue colour, the invading fluid (non-wetting) is red and the defending fluid (wetting) is a lighter shade of blue. In this case we wish to simulate a gravity flood so that we drive the fluid with a body force of 10^{-5} LB units. Solid boundary conditions are imposed on the left-hand and right-hand side-walls. The *x* dimension is 160 LB units and the *y* dimension is 120 LB units. The *z* direction thickness is only 6 LB units but we have periodic boundary conditions in this direction. We use a viscosity of 0.166 LB units for the non-wetting phase and 0.5 LB units for the wetting phase, giving a viscosity ratio of 3.

Figure 4b displays the flow at an intermediate time during the primary drainage flood. In the bottom left corner and the central region (near the inlet) there exist clusters of relatively large spheres. Thus the gap between these spheres is quite small and hence the capillary pressure required to invade these regions is large. As a result the invading fluid preferably floods the right hand side of the domain and the left central region. Thus two main fingers develop, which is typical of *viscous fingering*. As the flood proceeds the finger on the left side of the domain has the path of least resistance and hence rapidly reaches the outlet (Fig. 4c). The other finger, on the right side of the domain, has reached around 2/3 of the distance between inlet and outlet. It is clear from this simulation the interface between the non-wetting phase and wetting phase is unstable leading to viscous fingers which leave behind vast unexplored regions of the B-phase (blue), before reaching the outlet.

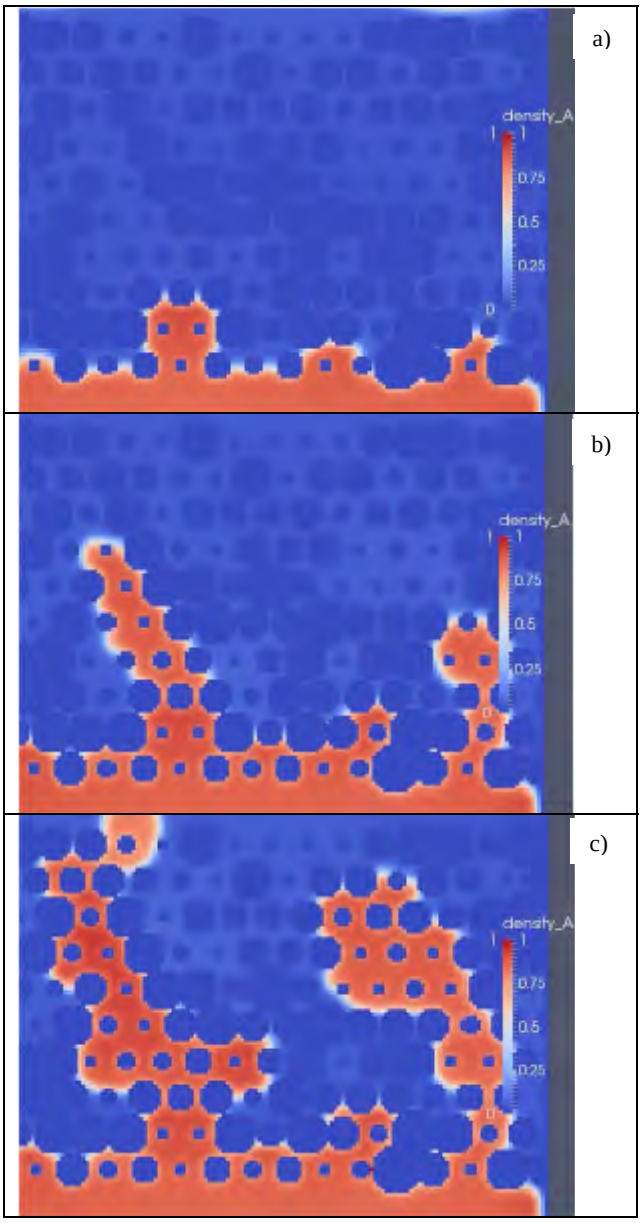

Figure 4. Two-phase immiscible displacement for a sample of packed spheres. A slice in the *x*-*y* plane is shown. The A-phase (red) is the non-wetting/invading fluid while the B-phase (blue) is the wetting/defending fluid. The dark blue spheres are solid. Fluid is driven by a constant body force of 10^{-5} LB units. a) Early configuration, b) intermediate configuration where non-wetting fluid preferentially fingers through domain and c) breakthrough configuration where non-wetting fluid has fingered through on two sides of the domain leaving behind regions of wetting fluid.

Carbonate Sample: The previous simulation has shown the present method yields a physically realistic realisation of a gravity driven flood in a packed bed. We now would like to apply it to a real rock sample. At the moment we do not have the computer memory and speed to complete a full 3D flood. So instead we apply the technique to a pseudo 3D geometry. We have obtained CT data of real carbonate rocks (Liu *et al*, 2014) and taken a slice of this data. That is a slice of dimension 400 voxels by 400 voxels and thickness of 6

voxels. Each voxel corresponds to a cube of edge length 2.9μm, so that the sample simulated is essentially 1.35mm^2 (with thickness in third dimension negligible). The porosity of this sample is high at around 55%.

One of the advantages of the LB method can be readily seen from Fig. 5, in that we simply input the CT data into our LB code. No pre-processing of the boundaries between solid and pore regions needs to be made, as in some other methods (Pereira *et al*, 2011). The flood in this case is driven by a body force of 10^{-5} LB units and solid boundary conditions are applied on the left and right-hand side walls. The same viscosities as for the packed bed case are used.

As in the packed bed case, the interface between non-wetting and wetting phases is unstable and leads to viscous fingers developing. These fingers rapidly invade the sample leaving behind unexplored regions of wetting phase. This will have significant implications on the overall recovery and relative permeability curves.

In principal, we can calculate relative permeability curves for this primary drainage flood using a single phase, multiple-relaxation time, LB method as we have previously done (Liu *et al*, 2014). At various stages during the flood, the configuration of each phase is input into the single phase code and permeabilities are calculated. In a realistic (three-dimensional) domain, one obtains non-zero permeabilities for each phase during the flood. However, in this simplified scenario, as soon the invading phase spans the width of the sample porous medium (e.g., see Fig. 4c) the defending phase permeability drops to zero. So the relative permeability curves become almost trivial. As such we do not display them for these cases.

CONCLUSIONS

The present work describes a numerical model for the complex process of multiphase flow in porous media. While we have focussed on applications in oil recovery, where the porous medium can have a highly irregular, random topology we also would like to apply this to other technological applications such as in micro or nano-fluidics. The present model is based on the Shan-Chen method but with an increased range of interaction which leads to an enhanced numerical stability of the algorithm. It has been shown to properly describe the behaviour of immiscible fluids leading to bubbles and droplets (either wetting or non-wetting) on solid substrates.

We have proceeded to apply the method to model immiscible flooding of porous media, which included packed beds and real rock samples. Both cases led to viscous fingering which results when the invading phase has a smaller viscosity than the defending phase and for comparatively large body forces. By varying these parameters (viscosity ratios and body forces) we would expect to recover other regimes of capillary fingering and stable displacement.

In spite of the encouraging results from this work, there still remain a few issues that remain to be addressed. These are:

- Implementation of a multi-relaxation time (MRT) scheme, yielding surface tensions which are independent of viscosity.
- Capability to deal with much larger three-dimensional domains, so as to model a real porous medium. This requires parallelisation of the present code.

These issues will be addressed in the future and results reported elsewhere.

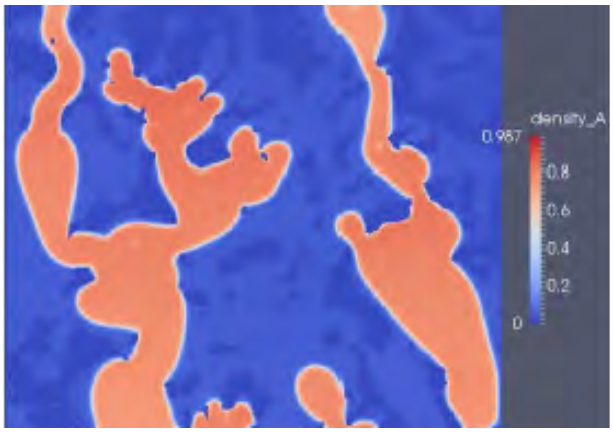

Figure 5. Breakthrough configuration in a carbonate sample. The invading (non-wetting) phase is red while the defending (wetting) phase is light blue. The solid regions are dark blue.

REFERENCES

BLUNT, M.J. (2001). "Flow in porous media - pore network models and multiphase flow". *Curr. Opin. Coll. Int Sci.*, **6**, 197-207.

CHEN, S. and DOOLEN, G.D. (1998). "Lattice Boltzmann method for fluid flows". *Ann. Rev. Fluid Mech.*, **30**, 329-364.

D'HUMIERES, D., GINZBURG, I., KRAFCZYK, M., LALLEMAND, P. and LUO, L.-S. (2002). "Multiple-relaxation-time lattice Boltzmann models in three dimensions". *Phil. Trans. R. Soc. Lond. A*, **360**, 437 - 451.

GUNSTENSEN, A.K. and ROTHMANN, D.H. (1992). "Lattice Boltzmann studies of immiscible two phase flow through porous media". *J. Geophys. Res*., **98**, 6431 - 6441.

HE, X., CHEN, S. and DOOLEN, G. (1998). "A novel thermal model for the lattice Boltzmann method in the incompressible limit". *J. Comput. Phys*., **146**, 282 - 300.

HUANG, H., THORNE, D.T., SCHAPP, M.G. and SUKOP, M.C. (2007). "Proposed approximation for contact angles in Shan-and-Chen-type multicomponent multiphase lattice Boltzmann models". *Phys. Rev. E*, **76**, 066701(1 - 6).

LIU, J., PEREIRA, G.G. and REGENAUER-LEIB, K. (2014). "From characterisation of pore structures to simulations of pore-scale fluid flow and the upscaling of permeability using microtomography: A case study of heterogeneous carbonates". *J. Geochem. Exp*., **144**, 84 -96.

PAN, C.X., LUO, L.S. and MILLER, C.T. (2006). “An evaluation of lattice Boltzmann schemes for porous medium flow simulations”. *Comp. and Fluids*, **35**, 898--909.

PEREIRA, G.G. (1999). “Numerical pore-scale modelling of three-phase fluid flow: Comparison between simulation and experiment”. *Phys. Rev. E*, **59**, 4229 - 4238.

PEREIRA, G.G., PRAKASH, M. and CLEARY, P. (2011). “SPH modelling of fluid at the grain level in a porous medium”. *App. Math. Modell.*, **35**, 166 - 175.

PORTER, M.L., E.T.COON, E.T., KANG, Q., MOULTON, J. and CAREY, J.W. (2012). “Multicomponent inter-particle potential lattice Boltzmann model for fluids with large viscosity ratios”. *Phys. Rev. E*, **86**, 036701(1 - 8).

SBRAGAGLIA, M., BENZI, R., BIFERALE, L., SUCCI, S., SUGIYAMA, S. and TOSCHI, F. (2007). “Generalized lattice Boltzmann method with multirange pseudopotential”. *Phys. Rev. E*, **75**, 026702(1 - 13).

SHAN, X. and CHEN, H. (1993). “Lattice Boltzmann model for simulating multiple phases and components”. *Phys. Rev. E, 47*, 1815 - 1819.

SUCCI, S. (2001). “The Lattice Boltzmann Equation for Fluid Dynamics and Beyond”. Oxford, UK.

SWIFT, M.R., OSBORN, W.R. and YOEMANS, J. (1995). “Lattice Boltzmann simulation of non-ideal fluids”. *Phys. Rev. Lett.*, **75**, 830 - 833.

ZOU, Q. and HE, X. (1997). “On pressure and velocity boundary conditions for the lattice Boltzmann BGK model”. *Phys. Fluids*, **9**, 1591 - 1598.